(Received 13 December 2024, Accepted 8 January 2025, Scheduled 15 January 2025)

Research on Constant Current Output Control of Wireless Power Transmission System Based on Parameter Identification

Zhongjiu Zheng, Yanpeng Ma*, Zhilong Wu, Xingfeng Cao, Qiangqiang Zhao, and Jinjun Bai

College of Marine Electrical Engineering, Dalian Maritime University, Dalian 116026, China

ABSTRACT: In the complex marine environment, the receiver is susceptible to the influence of water flow, which will cause the mutual inductance to fluctuate, thus affecting the stability of the output current. Therefore, aiming at the problem that the coil is prone to offset, this paper proposes a constant current charging output control method for a wireless power transmission system based on parameter identification. Firstly, a method of mutual inductance parameter identification is introduced in detail. Only by measuring the effective value of the current at the transmitting end, the equivalent equation of mutual inductance and current can be established. Aiming at solving complex mathematical equations, the results of mutual inductance identification are obtained from high-order equations by combining with particle swarm optimization algorithm. Secondly, on this basis, a constant current control method for fast calculation of the conduction angle based on the above identification method is proposed. The calculation process of the conduction angle is derived, and the working principle of the constant current charging control is introduced in detail. Finally, this paper completed the construction of the experimental platform and carried out relevant experimental verification. The results show that the error of the parameter identification method proposed in this paper is within 3%, and the constant current output control of the system can be realized in the case of mutual inductance disturbance.

1. INTRODUCTION

Underwater electromechanical equipment has shown very important application value in the fields of marine exploration, ocean development, and hydrological monitoring. As the main power source of underwater electromechanical equipment, the transmission mode of electric energy has become a major problem. The traditional underwater power transmission mainly adopts the wet insertion method, and the power is transmitted through the metal wire. The underwater environment will lead to corrosion and aging of metal wires, shortening the service life, and this wet plug interface has many disadvantages such as complex docking, high cost, and short service life.

Wireless Power Transfer (WPT) technology has gradually replaced some traditional power supply methods with the advantages of low maintenance cost, high reliability, and good waterproof [1–6]. However, underwater receiver is easy to shift with the influence of water flow, which will cause the mutual inductance to change, resulting in a sudden change in the charging current of the battery and reducing the service life of the battery. Therefore, it is necessary to study the constant-current (CC) charging control strategy.

In the current constant current control strategy, according to the position of the controller, it can be divided into transmitter control method and receiver control method. The control method of the receiving end is to add a DC/DC converter or use an active rectifier to realize the CC charging control of the system at the receiving end [7–11]. Receiving-side control can be performed without bilateral communication. However, on the one hand, DC/DC converters will increase the volume, weight, and cost of the receiving side. On the other hand, active rectification requires complex control methods and hardware circuits. However, for space-constrained Autonomous Underwater Vehicle (AUV), the receiver module should be as compact and lightweight as possible to achieve long mileage and high performance [12]. Therefore, compared with receiver control strategy, transmitter control strategy is more suitable for AUV and other underwater electrical equipment. When the primary side control is adopted, bilateral communication is usually required [13], but underwater communication is susceptible to electromagnetic interference and other effects. In order to solve this problem, people have carried out parameter identification without communication [14–20].

In [14], the mutual inductance value is estimated by measuring the input current value flowing through the inverter, the current value flowing through the transmitting coil, and the phase difference between the two, so as to adjust the conduction angle and realize the CC charging control of the system. This control strategy needs to design a circuit to calculate the phase difference, and the implementation process is more complicated. In [15], mutual inductance value is identified by pure mathematical analysis method, and the input voltage is adjusted to realize the CC charging control of the system when the mutual inductance changes from 13 μH to 17 μH. This control strategy depends on a large number of mathematical operations. In [16], charging current is inferred only by the electrical information at the transmitter, and then the CC charging control of the system is realized by using the shift control. This control strategy eliminates the traditional mutual inductance and load identification

* Corresponding author: Yanpeng Ma (a2802269239@dlmu.edu.cn).

process, but requires additional laminated magnetic couplers. In [17], mutual inductance decoupling is realized through circuit parameter design. On this basis, genetic algorithm is used to calculate the required operating frequency of CC charging, and constant current charging is realized by changing the operating frequency. In [18], non-communication mutual inductance identification is realized by making the system work at two non-resonant frequencies, and system CC charging control is realized on this basis. This strategy requires two frequencies and increases the workload. In [19], the charging state of the battery load is calculated according to the obtained voltage and current information of the transmitter, and the CC charging control of the system is realized by using the hybrid topology. In [20], the mutual inductance is identified by using the primary side detection circuit. On this basis, the two topologies are switched to realize the CC charging control of the system. However, the above method requires multiple control switches, which will increase the complexity of system control.

In transmitter control method, system CC charging is realized by adjusting the DC/DC duty cycle [21, 22] or system frequency [23, 24] and the phase shift angle of the full-bridge inverter [25, 26]. Transmitter control method can make up for the lack of space demand brought by the receiver control.

1) Duty cycle adjustment [21, 22]: In [21], bilateral synchronization is realized by extracting the switching frequency, and impedance tuning control is realized by adjusting the duty cycle of the DC/DC converter, so as to realize the system CC control. In [22], by adding a voltage stabilizing circuit at the transmitting end and switching the topology according to the mutual inductance value, the 10 W constant power output of the system is realized. During the experiment, the output power fluctuation of the system is within 5%. However, the above method requires additional circuits, which increases the cost, volume, and weight of the system.

2) Frequency regulation [23, 24]: In [23], two non-operating frequencies are used to supervise the mutual inductance in the front end, which reduces its sensitivity to parameter offset. Proportion Integral (PI) control is used to realize CC charging control. The equipment is simple, but it is suitable for static charging. In [24], by improving the genetic algorithm and setting up a penalty mechanism, the operating frequency of the system CC charging is solved, and system CC output is realized by changing the operating frequency. However, the disadvantage of frequency regulation is the need to replace different system frequencies, which makes system analysis and control complicated.

3) Phase shift control [25, 26]: In [25], by using wireless communication module, output voltage value is fed back to the transmitter, and then conduction angle is adjusted, so as to realize the CC charging control of the system. In [26], the radial basis function neural network is used to measure the load side current and change the conduction angle to realize the CC control of the system when the mutual inductance fluctuates rapidly. However, these control methods require bilateral communication.

In summary, in constant current charging control method, most of them need to use parameter identification, and the parameter identification process in the transmitter control method mostly requires bilateral communication. The wireless communication module will increase additional hardware and software costs. Therefore, this paper proposes a constant current output control method based on mutual inductance parameter identification. In the absence of communication, the mutual inductance value is identified, and on this basis, the inverter bridge shift angle is controlled to realize the system CC charging control. The main advantages of this paper are summarized as follows:

1) The parameter identification process in the control process does not require bilateral communication. It can be accurately estimated only by measuring the electrical quantity at the transmitter. This provides an idea for parameter identification in specific applications such as underwater and aerospace that are not suitable for wireless communication.

2) By controlling the conduction angle of the inverter, the CC charging control is realized; the voltage stabilizing circuit in the traditional system is reduced; the system cost is reduced; and the control process is simple.

3) Combined with particle swarm optimization algorithm, compared with the traditional particle swarm optimization algorithm method which needs to collect the current phase, the particle swarm identification in this paper does not need to collect the phase, eliminating the phase calculation circuit.

The rest of this article is as follows. In the second section, the system circuit model is established to analyze the influence of parameter changes on system performance. In the third section, the parameter identification process and constant current charging control method are introduced, and the identification results and control methods are verified by simulation. The fourth section gives experimental verification and analysis. Finally, the fifth section puts forward the conclusion.

2. CIRCUIT CHARACTERISTIC ANALYSIS OF WPT SYSTEM BASED ON LCC-S TOPOLOGY

In previous studies, four basic topologies have been widely used, among which S-S topology has been widely used because of its simple structure [26]. However, when the coil offset is too large, the S-S topology has overcurrent, which is not conducive to the safe operation of the system [27–30]. Therefore, people began to turn their attention to high-order topologies. LCC topology can avoid overcurrent when the mutual inductance decreases greatly, which ensures the safety of the system. Therefore, the LCC-S topology shown in Fig. 1 is selected in this paper, which consists of DC power supply V_{in}, controllable inverter bridge, topology, rectifier bridge, and load R_L.

In order to facilitate the system analysis, a simplified equivalent circuit is built as shown in Fig. 2. Among them, C_P, C_1, and C_s are compensation capacitors; L_p and L_s are the self-inductance of transmitting coil and receiving coil, respectively; R_{L1}, R_{Lp}, and R_{Ls} are the parasitic resistance of each coil. The mutual inductance between coils is M. The equivalent load is R, and the calculation formula of equivalent voltage source U_1

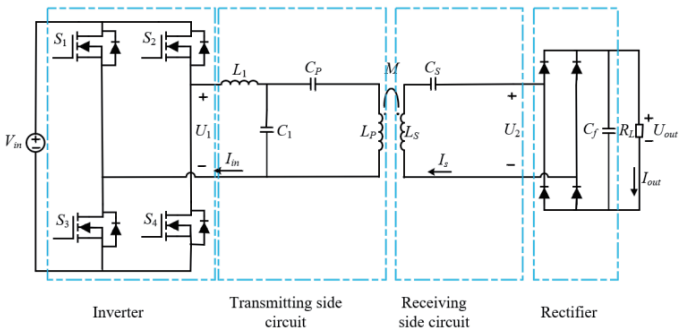

FIGURE 1. WPT system structure diagram.

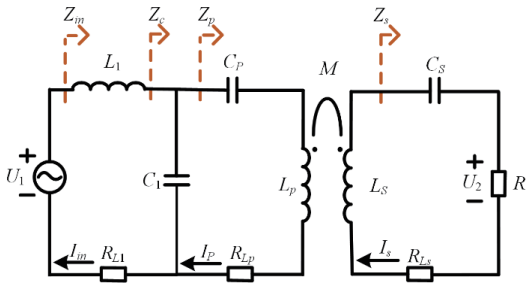

FIGURE 2. Fundamental equivalent circuit of LCC-S system.

TABLE 1. Electrical parameters of the system.

Parameter	L_p	R_{Lp}	L_s	R_{Ls}	C_p	C_1	C_s	L_1	R_L	U_{in}	f
Value	144 μH	109 mΩ	146 μH	100 mΩ	24 nF	103 nF	24 nF	34 μH	10 Ω	24 V	85 kHz

and equivalent load R is as follows:

$$U_1 = \frac{2\sqrt{2}}{\pi} U_{in} \sin\frac{\alpha}{2} \tag{1}$$

$$R = \frac{8}{\pi^2} R_L \tag{2}$$

where α is the conduction angle of the inverter. According to Kirchhoff's theorem, the circuit equation is written as follows:

$$\begin{cases} U_1 = (R_{L1} + j\omega L_1) I_{in} + \left(R_{Lp} + j\omega L_p + \dfrac{1}{j\omega C_P}\right) I_p \\ \qquad + j\omega M I_s \\ \left(R_{Lp} + j\omega L_p + \dfrac{1}{j\omega C_p}\right) I_p + j\omega M I_s = \dfrac{1}{j\omega C_1} (I_{in} - I_p) \\ -R_L' I_s = \left(R_{Ls} + j\omega L_s + \dfrac{1}{j\omega C_s}\right) I_s + j\omega M I_p \end{cases} \tag{3}$$

When the system resonates:

$$\omega = \frac{1}{\sqrt{L_1 C_1}} = \frac{1}{\sqrt{L_s C_s}} = \frac{1}{\sqrt{(L_p - L_1) C_p}} \tag{4}$$

Therefore, the output voltage, output power, and efficiency of the equivalent circuit are shown below [13]:

$$\begin{cases} A = R_{Lp} + \dfrac{(\omega M)^2}{R + R_{Ls}} + \dfrac{1}{(\omega C_1)^2 R_{L1}} \\ U_2 = \dfrac{M U_1 R}{C_1 R_{L1} (R + R_{Ls}) A} \\ P_{out} = \dfrac{(U_1 M)^2 R}{C_1^2 R_{L1}^2 (R + R_{Ls})^2 A^2} \\ \eta = \dfrac{(U_1 M)^2 R}{A (R + R_{Ls}) [\omega^2 C_1^2 R_{L1} A (R + R_{Ls}) - 1]} \end{cases} \tag{5}$$

Since the voltage in front of the rectifier bridge is a square wave, the output voltage and current to the load are as shown in (6):

$$\begin{cases} U_{out} = \dfrac{\pi\sqrt{2}}{4} U_2 \\ I_{out} = \dfrac{U_{out}}{R_L} \end{cases} \tag{6}$$

Starting from (5) and (6), when the system parameters are fixed, the output voltage and current of the system will be affected by M and R_L. In charging stage, it is mainly in the constant current charging stage. Therefore, according to the experimental platform, the experimental parameters shown in Table 1 are used to draw the curve of the output current of the WPT system with the mutual inductance of the coil and load as shown in Fig. 3.

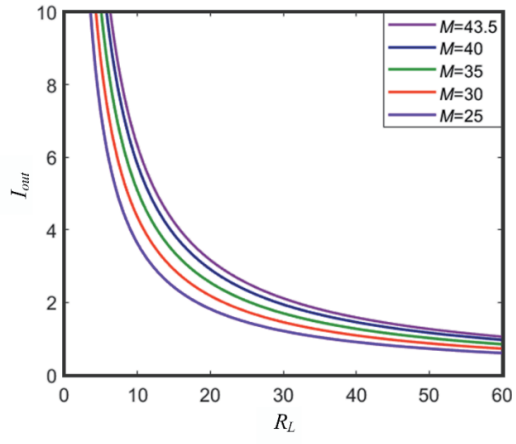

FIGURE 3. I_{out} varies with M and R_L.

It can be seen from Fig. 3 that when the system input voltage U_{in} and other parameters are fixed, the output current of the system increases with the increase of mutual inductance and decreases with the increase of load, which indicates that mutual

inductance and load have an important influence on the output current of the system. However, in the process of underwater charging, the charging equipment is more likely to be offset by factors such as water flow fluctuation, so that the mutual inductance is easy to change. Therefore, this paper mainly studies the CC charging control with mutual inductance disturbance.

3. CONTROL STRATEGY OF WPT SYSTEM BASED ON PARAMETER IDENTIFICATION

In order to realize CC charging control without communication, this paper adopts the control method based on mutual inductance parameter identification, and the control diagram is shown in Fig. 4. The working principle is as follows. Firstly, the input electrical information is collected for parameter identification. Secondly, the conduction angle corresponding to the constant current output is calculated according to the identification results. Finally, the current conduction angle is adjusted to the constant current conduction angle to realize the CC charging control of the system.

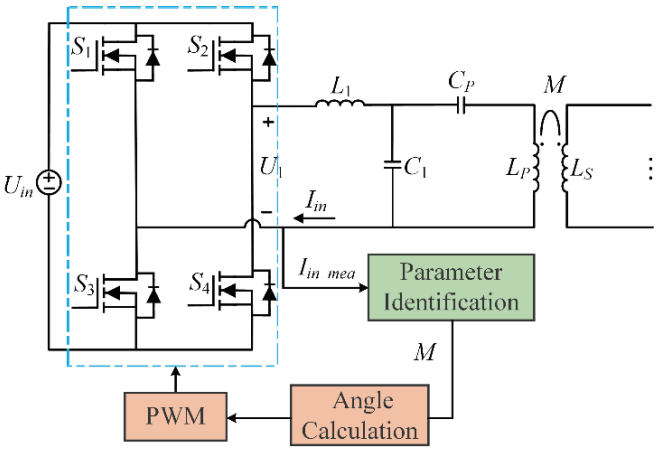

FIGURE 4. Schematic diagram of the proposed control strategy based on parameter identification.

3.1. Analysis of the Relationship Between $|I_{in}|$ and M

Starting from the equivalent circuit of Fig. 2, the equivalent impedance Z_s of the secondary side can be expressed as:

$$Z_s = R + R_{Ls} + j\omega L_s + \frac{1}{j\omega C_s} \tag{7}$$

The equivalent impedance Z_p can be expressed as:

$$Z_p = R_{Lp} + j\omega L_p + \frac{1}{j\omega C_p} + \frac{\omega^2 M^2}{Z_s} \tag{8}$$

The equivalent impedance Z_c can be expressed as:

$$Z_c = \frac{Z_p}{j\omega C_1 Z_p + 1} \tag{9}$$

The system input impedance Z_{in} can be expressed as:

$$Z_{in} = Z_c + j\omega L_1 + R_{L1} \tag{10}$$

Therefore, the system input current I_{in} can be expressed as:

$$I_{in} = \frac{U_{in}}{Z_{in}} \tag{11}$$

From (7) to (11), the functional relationship between the input current of the system and the mutual inductance between the coils is expressed as follows, where $|I_{in}|$ is the input current calculation modulus, X_{in} the imaginary part of Z_{in}, and R_{in} the real part of Z_{in}.

$$|I_{in}| = f(M) = \frac{U_{in}}{\sqrt{X_{in}^2 + R_{in}^2}} \tag{12}$$

Based on the trigonometric function, the current modulus is equal to the effective value, so the input current modulus can be measured by the actual circuit, which is I_{in_mea}. Further, the relationship between the input current and the mutual inductance and load is plotted as shown in Fig. 5, and the parameters used are shown in Table 1.

It can be seen from Fig. 5 that when the load is constant, the only mutual inductance value can be identified by measuring the effective value of the input current, so the parameter identification can be realized without communication. Further, because of the use of pure mathematical operations, the calculation process is complex, so in order to simplify the identification process, this paper uses the particle swarm optimization algorithm to solve it.

3.2. Tracking Based on Particle Swarm Optimization Algorithm

In the process of parameter identification, the fitness function of the traditional particle swarm optimization algorithm often needs to collect the current phase, which requires the design of additional phase calculation circuit, and when the system works at high frequency, the phase sampling accuracy will be challenged. Therefore, on this basis, this paper realizes the phase-independent parameter identification process by modifying its fitness function. The identification principle is shown in Fig. 6, and the specific control process is as follows:

1) Design population size, number of iterations and range;

2) Current effective value acquisition;

3) Calculate the fitness value of particles. The fitness function of this paper selects the error function of the effective value of the output current of the system model and identification model. The function expression is as follows:

$$e = |I_{in\_mea} - I_{in}(n)| \tag{13}$$

4) Compare the particle fitness value with the individual extreme value, and on this basis, compare with the group extreme value;

5) Update the speed and position, and deal with the boundary conditions.

$$w = (w_{\max} - w_{\min}) \frac{G - g}{G} + w_{\min} \tag{14}$$

(14) is the dynamic inertia weight coefficient formula, and $w_{\max}$ and $w_{\min}$ are the weights.

6) To determine whether the end. If yes, the output optimization results, otherwise return 3) continue to optimize.

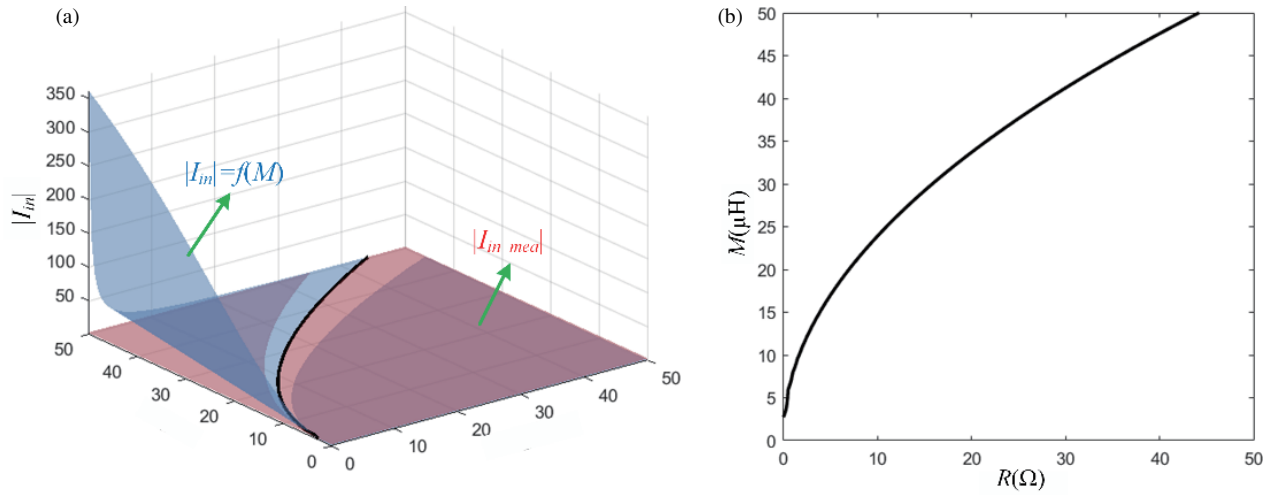

FIGURE 5. The relationship between I_{in} and (M, R): (a) Three-dimensional graph under 1.2 A constraint; (b) Top view under the constraint of 1.2 A.

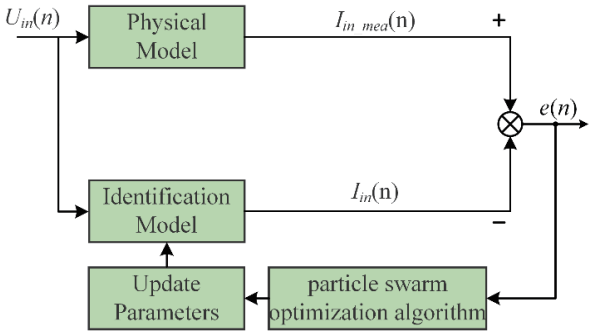

FIGURE 6. The principle diagram of parameter identification control strategy based on particle swarm optimization algorithm.

3.3. Novel Control Method Based on Fast Calculation of the Conduction Angle

When the mutual inductance is identified by the parameter identification method, the fast calculation of the conduction angle can be used to realize the CC charging control. The relationship between equivalent input voltage U_1 and equivalent output voltage U_2 can be obtained from (5) and (1), as shown in (15). By combining (1), (6), and (15), the sin $(\alpha/2)$ shown in (16) can be obtained. Furthermore, the conduction angle α of constant voltage charging can be expressed by (17), where α is the conduction angle of the inverter corresponding to the constant current output in the case of M disturbance.

$$U_1 = \frac{U_2 C_1 R_{L1}(R + R_{Ls})A}{MR} \tag{15}$$

$$\sin\left(\frac{\alpha}{2}\right) = \frac{\pi^2 C_1 R_{L1}\left(\frac{8R_L}{\pi^2} + R_{Ls}\right) A I_{out}}{8U_{in}M} \tag{16}$$

$$\alpha = 2 \cdot \arcsin\left(\frac{\pi^2 C_1 R_{L1}(\frac{8R_L}{\pi^2} + R_{Ls}) A I_{out}}{8U_{in}M}\right) \tag{17}$$

Further, according to the parameters of the experimental platform, the relationship between the output current and the mutual inductance and the conduction angle is obtained by using the parameters of Table 1, as shown in Fig. 7. In Fig. 7(a), the red plane is the 1.2 A target output current in the constant current charging control, and the blue surface is the relationship between the actual output current and the mutual inductance M and the conduction angle α. It can be found that there is a black common intersection line between the red plane and blue surface. This shows that a constant current output of 1.2 A can be achieved at any point on the black intersection into (17). In order to more clearly see the relationship between the two, Fig. 7(a) is projected onto the plane (M, α) to obtain the top view shown in Fig. 7(b). The black curve is the projection of the intersection of the red plane and blue surface. Starting from Fig. 7(b), in the case of known mutual inductance, the CC charging control of the system can be realized by changing the conduction angle of the inverter bridge required for CC charging.

In summary, the flowchart of the constant voltage output control method in this paper is shown in Fig. 8. The workflow of this paper is as follows:

1) Collect the input current I_{in} to identify the mutual inductance;

2) Bring the identification results into (17) to calculate the conduction angle α;

3) The driving circuit generates the corresponding target conduction angle according to the command signal, and performs CC charging control.

4. EXPERIMENTAL VERIFICATION

In order to further verify the feasibility of the proposed method, an experimental platform is built as shown in Fig. 9, and the parameter identification and constant current output are experimentally verified. The experimental platform includes DC power supply module, single bridge inverter and drive power supply, DSP control unit, primary and secondary compensation network, acquisition module, transmitting and receiving coils, uncontrollable rectifier bridge module, electronic load, etc. The electrical parameters of the system are shown in Table 1.

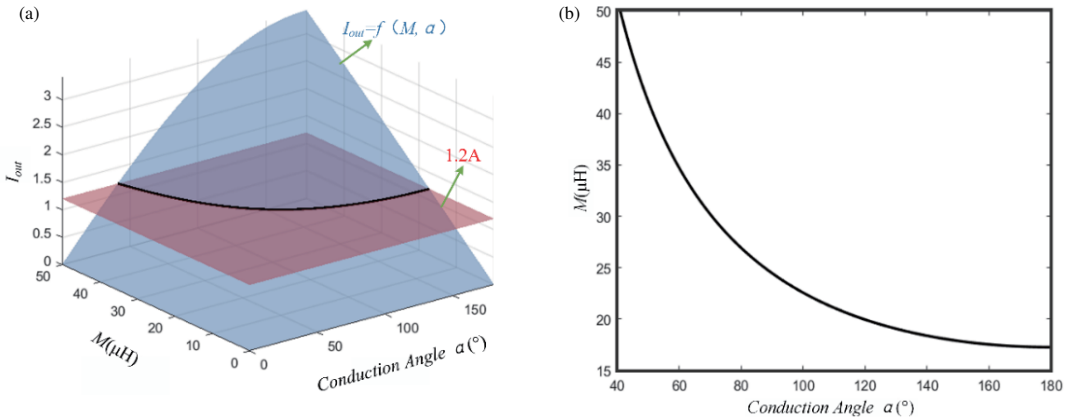

FIGURE 7. The relationship between the output current and (M, α): (a) Three-dimensional graph under 1.2 A constraint; (b) Top view under the constraint of 1.2 A.

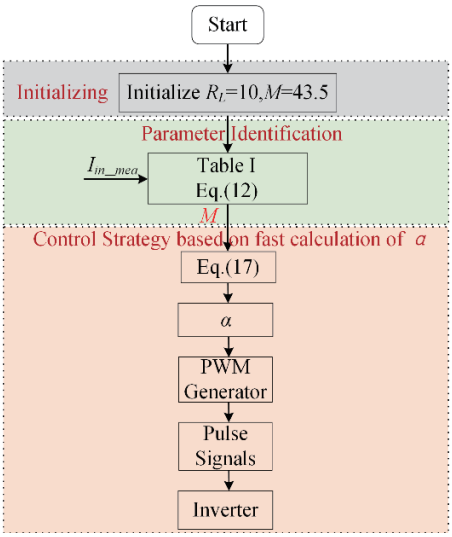

FIGURE 8. Flowchart of CC output control strategy based on parameter identification.

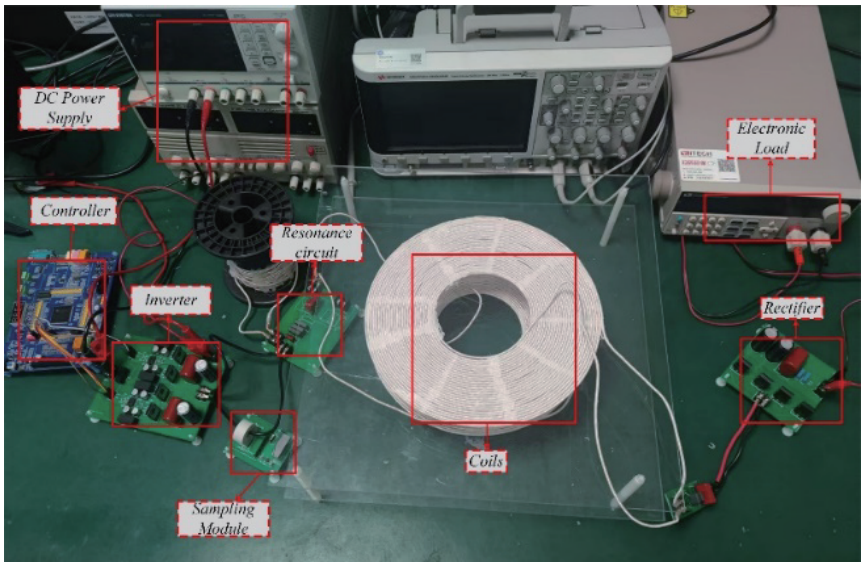

FIGURE 9. Experimental platform.

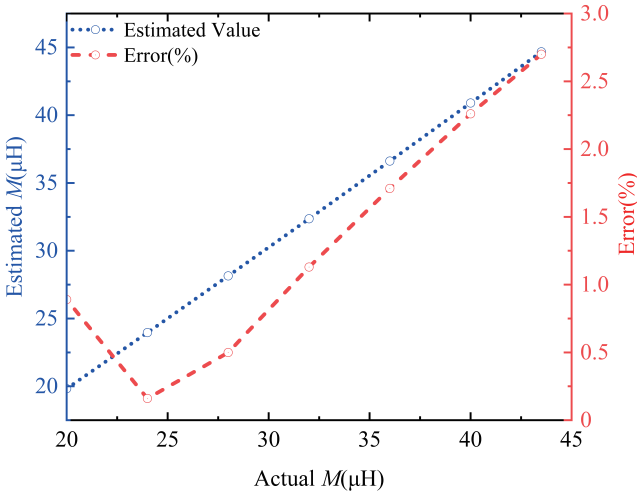

FIGURE 10. The identification result of M.

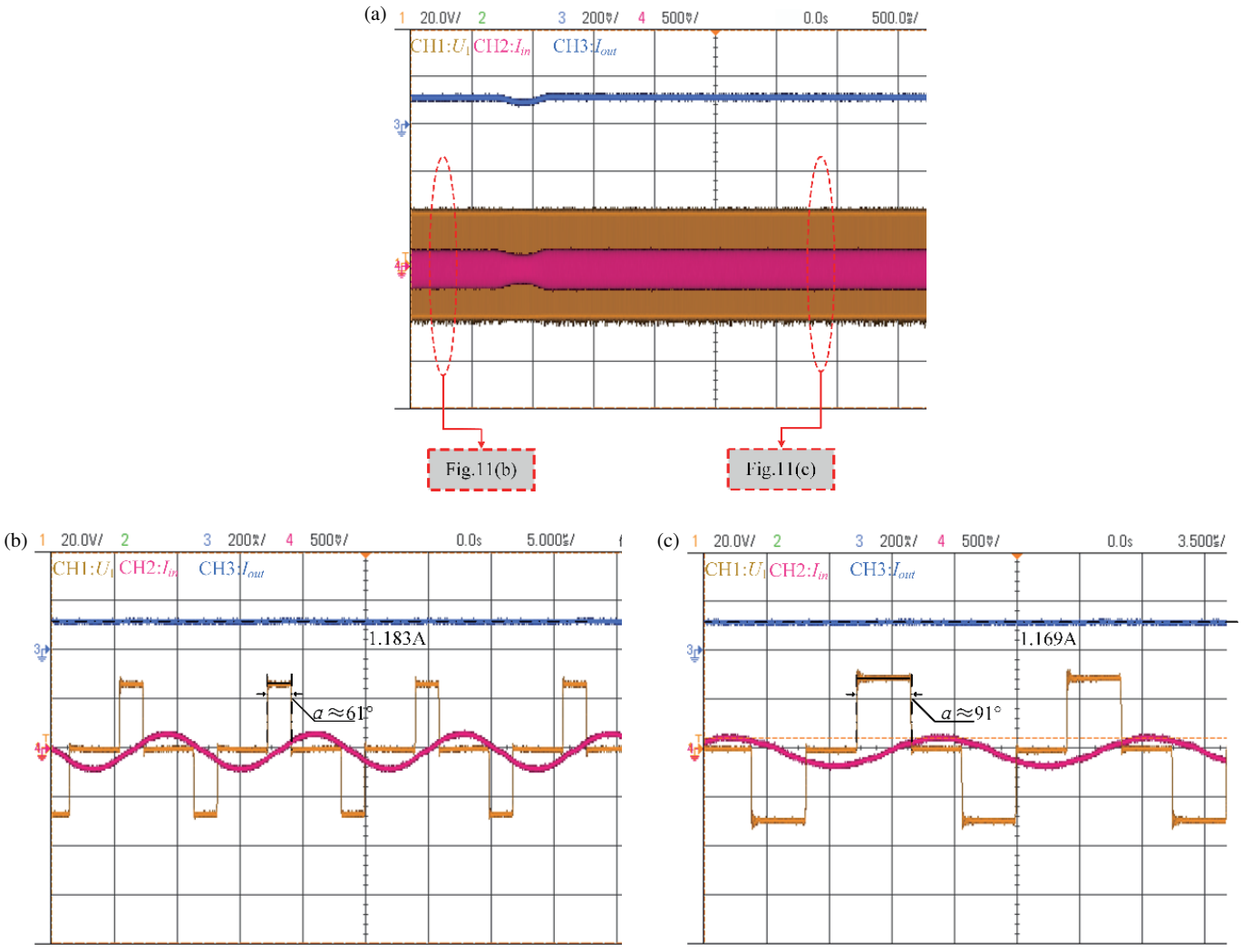

FIGURE 11. When $R = 10\,\Omega$, the output and conduction angle corresponding to different M: (a) $M = 26\,\mu H$ to $37\,\mu H$; (b) $M = 26\,\mu H$; (c) $M = 37\,\mu H$.

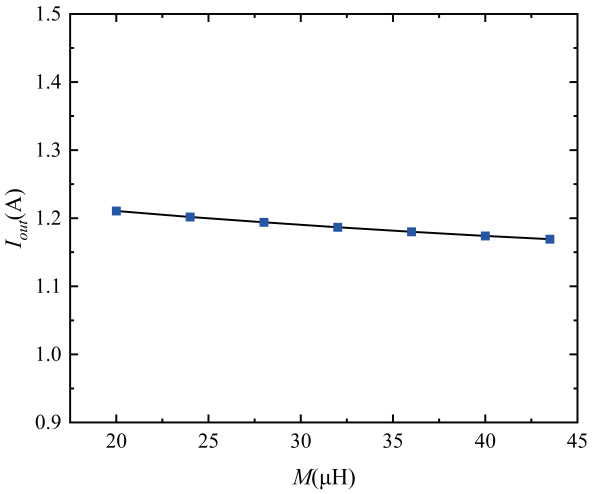

FIGURE 12. Current output under different mutual inductance states.

4.1. Parameter Identification Verification

In order to verify the accuracy of parameter identification, this paper experimentally verifies the two topologies under different horizontal offsets. Fig. 10 shows the comparison between the estimated mutual inductance value and real mutual inductance value under different horizontal offsets, where the blue curve is the mutual inductance estimated by parameter identification, and the red curve is the estimation error. It can be seen from Fig. 10 that the estimated value is close to the real value, and the maximum error is 2.7%. The reason for the error may be the change of electrical parameters caused by the measurement error and offset of some electrical parameters, such as the inductance value of the coil and the inductance value and capacitance value of the compensation network, and the fluctuation of the self-inductance of the transmitting coil during the offset process. At the same time, the measurement deviation of WPT primary side electrical may also be one of the reasons, so the parameter identification method has good accuracy in the case of coil offset.

4.2. Constant Current Control Verification

In order to verify the accuracy of the constant voltage control method proposed in this paper, the experimental load is set to 10 Ω, and the proposed method is experimentally verified under different offset conditions. The experimental results are shown in Fig. 11. In Fig. 11(a), the change of the electrical information of the system is shown when the mutual inductance changes from 26 μH to 37 μH. Among them, the blue line is the load charging current, and the orange curve and purple curve are the input voltage and current of the inverter, respectively. Further, in order to more clearly see the changes in the amount of electrical information, the changes in the amount of electrical information when the mutual inductance is 26 μH and 37 μH are shown in Fig. 11(b) and Fig. 11(c). From Fig. 11(b) and Fig. 11(c), it can be seen that by adjusting the conduction angle to 91° and 61°, the system current fluctuation can be controlled within 3%.

Further, the output current changes of the system under different coil offsets are obtained as shown in Fig. 12. From Fig. 12, it can be seen that in the case of different mutual inductances, the output current fluctuation rate of the system can be controlled within 3% by applying the constant voltage control method in this paper, which fully proves the feasibility of the constant current output control method based on mutual inductance parameter identification proposed in this paper.

5. CONCLUSION

In order to enhance the anti-offset ability of underwater wireless power transmission system, this paper proposes a constant current output control method for underwater wireless power transmission system based on mutual inductance parameter identification. By introducing current mode into particle swarm optimization algorithm, the mutual inductance parameter identification with an error within 2.7% is realized. On this basis, through the shift constant current output control, the system output current fluctuation can be achieved within 3% when the coil is offset due to factors such as water flow fluctuation. Therefore, the method in this paper can effectively improve the anti-offset ability of the system and provide an effective solution to the constant current control problem of the underwater WPT system.

ACKNOWLEDGEMENT

On behalf of all authors, the corresponding author states that there is no conflict of interest.

REFERENCES

[1] Hu, J., J. Zhao, and F. Gao, "A real-time maximum efficiency tracking for wireless power transfer systems based on harmonic-informatization," *IEEE Transactions on Power Electronics*, Vol. 38, No. 1, 1275–1287, Jan. 2023.

[2] Cai, J., X. Wu, P. Sun, Q. Deng, J. Sun, and H. Zhou, "Design of constant-voltage and constant-current output modes of double-sided LCC inductive power transfer system for variable coupling conditions," *IEEE Transactions on Power Electronics*, Vol. 39, No. 1, 1676–1689, Jan. 2024.

[3] Zeng, J., J. Wu, K. Li, Y. Yang, and S. Y. R. Hui, "Dynamic monitoring of battery variables and mutual inductance for primary-side control of a wireless charging system," *IEEE Transactions on Industrial Electronics*, Vol. 71, No. 7, 7966–7974, Jul. 2024.

[4] Cai, C., J. Wang, Y. Luo, Y. Rao, P. Zhang, T. Zang, H. Lin, and L. Liu, "Multistate voltage balancing of UAV's cell string: A reconfigurable WPT-based multiport hybrid charging approach," *IEEE Transactions on Industrial Electronics*, Vol. 72, No. 1, 266–277, Jan. 2025.

[5] Jia, Y., L. Zhao, Z. Wang, C. Tang, F. Chen, and H. Feng, "Integrated LCC-LCC topology for WPT system with CC output regarding air gap and load variations," *IEEE Transactions on Power Electronics*, Vol. 39, No. 10, 11 904–11 915, Oct. 2024.

[6] Wang, J., S. Yu, Y. Huang, B. Lin, G. Liang, X. Xie, and C. Xie, "Communication-free long-distance wireless charging system for battery load with adaptive switching of constant voltage and constant current," *IEEE Transactions on Transportation Electrification*, Vol. 10, No. 2, 2653–2662, Jun. 2024.

[7] He, H., S. Wang, Y. Liu, C. Jiang, X. Wu, B. Wei, and B. Jiang, "Maximum efficiency tracking for dynamic WPT system based on optimal input voltage matching," *IEEE Access*, Vol. 8, 215 224–215 234, 2020.

[8] Guo, Y. and Y. Zhang, "Secondary side voltage and current estimation of wireless power transfer systems," *IEEE Transactions on Industry Applications*, Vol. 58, No. 1, 1222–1230, Jan.-Feb. 2022.

[9] Li, Z., C. Zhu, J. Jiang, K. Song, and G. Wei, "A 3-kW wireless power transfer system for sightseeing car supercapacitor charge," *IEEE Transactions on Power Electronics*, Vol. 32, No. 5, 3301–3316, 2017.

[10] Zhong, W. X. and S. Y. R. Hui, "Maximum energy efficiency tracking for wireless power transfer systems," *IEEE Transactions on Power Electronics*, Vol. 30, No. 7, 4025–4034, 2015.

[11] Yang, Y., W. Zhong, S. Kiratipongvoot, S.-C. Tan, and S. Y. R. Hui, "Dynamic improvement of series-series compensated wireless power transfer systems using discrete sliding mode control," *IEEE Transactions on Power Electronics*, Vol. 33, No. 7, 6351–6360, Jul. 2018.

[12] Cheng, Z., Y. Lei, K. Song, and C. Zhu, "Design and loss analysis of loosely coupled transformer for an underwater high-power inductive power transfer system," *IEEE Transactions on Magnetics*, Vol. 51, No. 7, 1–10, Jul. 2015.

[13] Fu, N., J. Deng, Z. Wang, and D. Chen, "Dual-phase-shift control strategy with switch-controlled capacitor for overall efficiency optimization in wireless power transfer system," *IEEE Transactions on Vehicular Technology*, Vol. 72, No. 6, 7304–7317, Jun. 2023.

[14] Gu, Y., J. Wang, Z. Liang, and Z. Zhang, "Mutual-inductance-dynamic-predicted constant current control of LCC-P compensation network for drone wireless in-flight charging," *IEEE Transactions on Industrial Electronics*, Vol. 69, No. 12, 12 710–12 719, Dec. 2022.

[15] Zhang, K., W. Gao, R. Shi, Z. Yan, B. Song, and A. P. Hu, "An impedance matching network tuning method for constant current output under mutual inductance and load variation of IPT system," *IEEE Transactions on Power Electronics*, Vol. 35, No. 10, 11 108–11 118, Oct. 2020.

[16] Li, Z., H. Liu, Y. Tian, and Y. Liu, "Constant current/voltage charging for primary-side controlled wireless charging system without using dual-side communication," *IEEE Transactions on Power Electronics*, Vol. 36, No. 12, 13 562–13 577, Dec. 2021.

[17] Cai, J., X. Wu, P. Sun, Q. Deng, J. Sun, and H. Zhou, "Design of constant-voltage and constant-current output modes of double-sided LCC inductive power transfer system for variable coupling conditions," *IEEE Transactions on Power Electronics*, Vol. 39, No. 1, 1676–1689, Jan. 2024.

[18] Mao, Y., Y. Yang, and K. Wang, "A primary-side fixed-frequency CC and CV output control for single-stage wireless battery chargers with series compensation receivers," *IEEE Transactions on Transportation Electrification*, Vol. 10, No. 2, 3407–3415, Jun. 2024.

[19] Wang, J., S. Yu, Y. Huang, B. Lin, G. Liang, X. Xie, and C. Xie, "Communication-free long-distance wireless charging system for battery load with adaptive switching of constant voltage and constant current," *IEEE Transactions on Transportation Electrification*, Vol. 10, No. 2, 2653–2662, Jun. 2024.

[20] Li, X., H. Wang, F. Zheng, X. Dai, Y. Sun, and A. P. Hu, "Wireless charging of substation inspection robots based on parameter estimation without communication," *IEEE Transactions on Circuits and Systems II: Express Briefs*, Vol. 71, No. 2, 907–911, Feb. 2024.

[21] Ann, S. and B. K. Lee, "Analysis of impedance tuning control and synchronous switching technique for a semibridgeless active rectifier in inductive power transfer systems for electric vehicles," *IEEE Transactions on Power Electronics*, Vol. 36, No. 8, 8786–8798, Aug. 2021.

[22] Li, Z., B. Xie, Y. Zhu, M. Tang, H. Liu, X. Guo, and H. Sun, "Wireless charging constant power output system based on LCC/SS self-switching," *IEEE Access*, Vol. 10, 86 435–86 444, 2022.

[23] Mao, Y., Y. Yang, and K. Wang, "A primary-side fixed-frequency CC and CV output control for single-stage wireless battery chargers with series compensation receivers," *IEEE Transactions on Transportation Electrification*, Vol. 10, No. 2, 3407–3415, Jun. 2024.

[24] Cai, J., X. Wu, P. Sun, Q. Deng, J. Sun, and H. Zhou, "Design of constant-voltage and constant-current output modes of double-sided LCC inductive power transfer system for variable coupling conditions," *IEEE Transactions on Power Electronics*, Vol. 39, No. 1, 1676–1689, Jan. 2024.

[25] Wei, Y. and F. Wu, "Indirect control strategy of secondary current for LCC-series compensated wireless power transfer system based on primary current closed-loop control," *IEEE Transactions on Transportation Electrification*, Vol. 8, No. 2, 1553–1565, Jun. 2022.

[26] Zhang, Z., S. Shen, Z. Liang, S. H. K. Eder, and R. Kennel, "Dynamic-balancing robust current control for wireless drone-in-flight charging," *IEEE Transactions on Power Electronics*, Vol. 37, No. 3, 3626–3635, Mar. 2022.

[27] She, Z., S. Chen, Y. Chen, Y. Zhang, H. Li, and Y. Tang, "Efficiency analysis of LCC-S and SS inductive power transfer considering switching device and component losses," in *2020 IEEE 9th International Power Electronics and Motion Control Conference (IPEMC2020-ECCE Asia)*, 2956–2960, Nanjing, China, 2020.

[28] Yang, L., S. Jiang, C. Wang, Y. Shi, M. Wang, C. Cai, and L. Zhang, "A high-efficiency integrated LCC/S WPT system with constant current output," *IEEE Journal of Emerging and Selected Topics in Power Electronics*, Vol. 12, No. 1, 341–354, Feb. 2024.

[29] Zhang, R., H. Yuan, M. Rong, W. Ke, C. Liang, J. Chu, A. Yang, W. Huang, G. Huang, and X. Wang, "Self-tuning wpt system with constant voltage output under resonance frequency shift," *IEEE Transactions on Power Electronics*, Vol. 39, No. 1, 1713–1722, Jan. 2024.

[30] Li, M., J. Deng, D. Chen, W. Wang, Y. Li, and Z. Wang, "A minimum ZVS current control strategy of semi bridgeless active rectifier for wide operation range based on LCC-S compensated WPT system," *IEEE Transactions on Industry Applications*, Vol. 59, No. 3, 3481–3492, May-Jun. 2023.